LA-UR- 99-3111

Approved for public release; distribution is unlimited.

Title: Huygens-Fresnel Wave Optics Simulation of atospheric Optrical Turbulence and Reflective Speckle in CO2 Differential Absorption Lidar (DIAL)

Author(s):

Douglas Nelson, CST-1
Roger Petrin, CST-1
Edward MacKerrow, XCM
Mark Schmitt, XCM
Bernard Foy, CST-6
Aaron Koskelo, CST-1
Brian McVey, XCM
Charles Quick, CST-1
William Porch, EES-8
Joe Tiee, CST-6
Charles Fite, NIS-3
Frank Archuleta, CST-1
Michael Whitehead, CST-6
Donald Walters, Naval Postgd
L. John Jolin, CST-6

Submitted to:

SPIE Annual Meeting
July 18-23, 1999
Denver, CO

Los Alamos
NATIONAL LABORATORY

DISCLAIMER

DISCLAIMER

Portions of this document may be illegible in electronic image products. Images are produced from the best available original document.

Huygens-Fresnel wave-optics simulation of atmospheric optical turbulence and reflective speckle in CO_2 differential absorption lidar (DIAL)

Douglas H. Nelson[a], Roger R. Petrin[a], Charles R. Quick[b], L. John Jolin[a], Edward P. MacKerrow[a], Mark J. Schmitt[a], Bernard R. Foy[a], Aaron C. Koskelo[b], Brian D. McVey[a], William M. Porch[c], Joe J. Tiee[a], Charles B. Fite[d], Frank A. Archuleta[a], Michael C. Whitehead[e] and Donald L. Walters[f]

[a]Los Alamos National Laboratory, MS E543, Los Alamos, NM 87545
[b]Los Alamos National Laboratory, MS J565, Los Alamos, NM 87545
[c]Los Alamos National Laboratory, MS D407, Los Alamos, NM 87545
[d]Los Alamos National Laboratory, MS D440, Los Alamos, NM 87545
[e]Los Alamos National Laboratory, MS J567, Los Alamos, NM 87545
[f]Naval Postgraduate School, Code PH/We, Monterey, CA 93943

ABSTRACT

The measurement sensitivity of CO_2 differential absorption LIDAR (DIAL) can be affected by a number of different processes. Two of these processes are atmospheric optical turbulence and reflective speckle. Atmospheric optical turbulence affects the beam distribution of energy and phase on target. The effects of this phenomenon include beam spreading, beam wander and scintillation which can result in increased shot-to-shot signal noise. In addition, reflective speckle alone has been shown to have a major impact on the sensitivity of CO_2 DIAL. We have previously developed a Huygens-Fresnel wave optics propagation code to separately simulate the effects of these two processes. However, in real DIAL systems it is a combination of these phenomena, the interaction of atmospheric optical turbulence and reflective speckle, that influences the results. In this work, we briefly review a description of our model including the limitations along with a brief summary of previous simulations of individual effects. The performance of our modified code with respect to experimental measurements affected by atmospheric optical turbulence and reflective speckle is examined. The results of computer simulations are directly compared with lidar measurements and show good agreement. In addition, simulation studies have been performed to demonstrate the utility and limitations of our model. Examples presented include assessing the effects for different array sizes on model limitations and effects of varying propagation step sizes on intensity enhancements and intensity probability distributions in the receiver plane.

Keywords: atmospheric turbulence, laser speckle, beam propagation

1. INTRODUCTION

The geometry of a hard target reflection scheme is shown in Figure 1. As the laser beam propagates toward the target, index of refraction fluctuations in the atmosphere cause phase distortions in the transverse electric field distribution. Once the laser beam reaches the target, its spatial intensity distribution has been altered compared to what would be observed in propagating through a vacuum. At the target, light is scattered back toward the transmitter. This light passes through essentially the same turbulent atmosphere that altered the outgoing beam (since the atmosphere is "frozen" during the transit time of the pulse for our typical lidar geometries). The return signal will be reduced by any manmade absorbing species in the path in accordance with Beer's law. Absorption will also occur from normal atmospheric constituents.

We have developed a Huygens-Fresnel wave optics propagation code to simulate the effects of reflective speckle and atmospheric optical turbulence. Previously, we compared the ability of our model to predict these separate effects with a combination of theory and experimental observations. [1,2] However, in real DIAL systems it is a combination of these phenomena, the interaction of atmospheric optical turbulence and reflective speckle, which influences the results.[3] We present preliminary results of the comparison of our combined effects simulation with experimental measurements over a finite aperture. We have conducted simulation studies to determine the nature of the reflective speckle-atmospheric turbulence interaction and examine model limitations.

2. MODEL

The model employs the Fresnel-Kirchoff theorem with the Fresnel approximation and assumes paraxial, on-axis propagation.[4,5] This model is applied to a lidar geometry in which the beam propagates from the transmitter/receiver through an optically turbulent atmosphere to a diffuse hard target. The atmospheric optical turbulence effects are approximated by a series of phase screens over several propagation steps.[6,7] To simulate reflection from a diffuse hard target, we randomize the phase. After scattering from the target, the portion of the beam that reflects back to our receiver propagates along the same optically turbulent path.

Our Huygens-Fresnel wave optics simulation uses an $N \times N$ array of complex numbers to represent the electric field in a plane perpendicular to the propagation axis. The initial electric field, a Gaussian TEM_{00} spatial intensity and phase distribution with the properties of our experimental transmitter beam, is used as the input for the simulation. The simulation propagates this initial electric field by dividing the path from lidar system to the target into equal sized steps and applying a phase screen to simulate turbulence effects at each step. The expression for the electric field after a step of distance Δz is determined from[7]

$$E(\hat{\rho},\Delta z) = IFT\left[\exp\left(i\cdot\pi\cdot\lambda\cdot\Delta z\cdot\left|\hat{f}\right|^2\right)\cdot FT\left[E(\hat{\rho},0)\cdot\exp\{i\cdot\theta(\hat{\rho})\}\right]\right], \qquad (1)$$

where $E(\hat{\rho},0)$ is the electric field at the initial portion of the step ($z = 0$) with the transverse coordinate given by $\hat{\rho}$. FT is the discrete two-dimensional Fourier transform, $\exp\left(i\cdot\pi\cdot\lambda\cdot\Delta z\cdot\left|\hat{f}\right|^2\right)$ is the Fresnel propagator in the spatial frequency domain $\hat{f}$, λ is the laser wavelength and IFT is the discrete two-dimensional *inverse* Fourier transform. The phase screen, $\theta(\hat{\rho})$, is[6,7]

$$\theta(\hat{\rho}) = 0.0984\cdot k_o\cdot\sqrt{C_n^2(z)\cdot\Delta z}\cdot(N\cdot\delta x)^{5/6}\,FT\left[\left(\sqrt{n_x^2+n_y^2}\right)^{-11/6}\cdot\Theta_o(n_x,n_y)\right], \qquad (2)$$

where $k_o = 2\pi/\lambda$, $C_n^2(z)$ is the path dependent index of refraction structure constant which characterizes the level of turbulence[8], Δz is again the step propagation distance, N is the number of pixels along one dimension of the transverse array, $\delta x = \sqrt{\lambda L/N}$ is the optimized pixel width for a transmitter-to-hard target distance of L, n_x and n_y denote integer pixel coordinates within the two-dimensional transverse array, $\Theta_o(n_x,n_y)$ represents an $N \times N$ array of complex unit-variance Gaussian random numbers and FT again implies the two-dimensional discrete Fourier transform. The argument of the FT operation is an array in the spatial frequency domain produced by taking a Gaussian random number distribution and applying the $\left(\sqrt{n_x^2+n_y^2}\right)^{-11/6}$ factor to impose properties of the Kolmogorov spectrum, which describes the spatial frequency distribution of index of refraction fluctuations, in the transverse plane.[9] As seen in Equation (2), the magnitude of the turbulence induced phase is dependent on the strength of the turbulence, the length of the propagation step and the lidar wavelength.

The number of propagation steps has a direct impact on computation time. To keep this computation time at a minimum, one goal is to keep the number of propagation steps as low as possible. However, our model is limited in that there are constraints on propagation step size. The assumptions used to approximate a propagation step dictate that the step be within the near field propagation distance. For our lidar geometry, this means that the step can be no longer than the Rayleigh range of our laser transmitter.

There is another free space limit on the size of a propagation step one may use in the split-step method. The shortest step or maximum number of steps can be determined by considering the approximation of phase that led to propagation relation Equation (1). This approximation was applied to an expression of the Fresnel-Kirchoff theorem

$$E(\hat{r},z) \approx -\frac{i}{\lambda z}\int E(\hat{\rho},0)\exp\left\{\frac{i2\pi z}{\lambda}\sqrt{1+\left|\frac{\hat{r}-\hat{\rho}}{z}\right|^2}\right\}d\hat{\rho}, \quad (3)$$

and begins with a binomial expansion of the radical in the exponential argument. This expansion takes the form

$$\sqrt{1+b} = 1+\frac{1}{2}b+\frac{1}{8}b^2+\ldots, \quad (4)$$

where $|b|<1$ and b is given by

$$b = \left|\frac{\hat{r}-\hat{\rho}}{z}\right|^2. \quad (5)$$

The approximation assumes that terms of order b^2 and higher may be neglected. To determine the maximum number of steps one may use, assume that the b^2 term is two orders of magnitude smaller than the b term

$$\frac{1}{2}b \cong 100\frac{1}{8}b^2. \quad (6)$$

Using the expression for b and assuming that the maximum separation distance between $\hat{r}$ and $\hat{\rho}$ is on the order of the transverse grid size $N\delta x$ for a propagation step size Δz

$$b = \left|\frac{\hat{r}-\hat{\rho}}{\Delta z}\right|^2 \cong \left(\frac{N\delta x}{\Delta z}\right)^2 \cong \frac{1}{25}. \quad (7)$$

Substituting the expression for the optimized pixel size δx

$$\delta x = \sqrt{\frac{\lambda \cdot L}{N}}, \quad (8)$$

the maximum number of steps, $\#steps$, for a given array size $N\times N$, total propagation distance L and transmitter wavelength λ is

$$\#steps \cong \sqrt{\frac{L}{25N\lambda}}. \quad (9)$$

From this relationship, the number of steps decreases as the array size $N\times N$ increases. Larger arrays therefore provide better transverse spatial resolution at a cost of longitudinal spatial resolution.

Another constraint is that phase effects over this step must not be dominated by amplitude effects. Martin and Flatté [10] found that for the phase screen approach to be valid, the normalized point irradiance, σ_I^2, defined below, for a single propagation step must be less than $1/10$ of the total normalized point irradiance variance for the total propagation distance, L,

$$\sigma_I^2(\Delta z) < 0.1\sigma_I^2(L). \quad (10)$$

In addition, they found that this variance must be less than 0.1 for one step

$$\sigma_I^2(\Delta z) < 0.1. \quad (11)$$

For spherical wave propagation, assuming weak turbulence, the RMS noise or scintillation at an on-axis point detector is[11]

$$\sigma_{\bar{I}} = \sqrt{\exp(4\sigma_\chi^2)-1}, \quad (12)$$

where $\sigma_{\bar{I}} = \sigma_I/\bar{I}$ is the normalized standard deviation of irradiance. This is the square root of the normalized point irradiance variance discussed earlier. The value σ_χ^2 is the spherical wave log amplitude variance for a point detector. For a

path of length L with uniform turbulence along the entire path (i.e. constant turbulence level - C_n^2) the spherical wave log amplitude variance is[8]

$$\sigma_\chi^2 = 0.124 C_n^2 k_o^{7/6} L^{11/6}, \quad (13)$$

again with $k_o = 2\pi/\lambda$.

3. SIMULATION OF INDIVIDUAL EFFECTS

We have shown that this model works well predicting separately the effects of atmospheric optical turbulence and reflective speckle.[1,2] The simulation of long-term turbulent beam spreading was found to be in agreement with both experimental data and analytical predictions. Simulation values for point detector scintillation due to atmospheric optical turbulence showed agreement with analytical predictions.

We also considered separately the reflective speckle effects in the absence of atmospheric optical turbulence.[1,2] A surface that is rough on the scale of the laser wavelength scatters the coherent lidar pulse, which produces a complex interference pattern.[12] This pattern is granular in appearance and is commonly referred to as a speckle pattern. Simulated speckle coherence or correlation "sizes" were found to be in excellent agreement with those predicted by theory. The intensity probability distributions predicted by our simulation for circular receiver apertures of varying radii agreed with those observed in experiment and expected from theory. These probability distributions are characterized by the parameter *M*, which is interpreted as the number of speckle inside the receiver for an average pulse. We compared these *M* values to geometrical predictions from the ratio of the receiver aperture area to the estimated speckle correlation area. We also compared the *M* values from these probability distributions to the signal-to-noise ratio obtained from the simulation. The simulated intensity probability distributions and *M* value were consistent with those measured experimentally.[13]

4. COMBINED EFFECTS SIMULATION AND COMPARISON WITH EXPERIMENT

We conducted experiments during June and July 1998 in the Nevada desert under conditions of diurnally varying levels of atmospheric turbulence (C_n^2) at ranges of 1360 m and 2160 m. The target at 1360 m was a rotating drum with a diffuse surface. This rotating drum target was specifically designed to provide independent speckle realizations as the drum turns at ~ 2 revolutions per minute. The target at 2160 m had a diffuse surface fixed to plywood. Our lidar consisted of a CO_2 laser with an effective pulse rate per line of 113 Hz. The receiver configuration was annular with an inner diameter of 4.65" and an outer diameter of 12". The propagation path was horizontal over flat, featureless desert terrain. We concurrently measured the turbulence level with an incoherent near infrared scintillometer propagating over a path that was approximately parallel azimuthally to our lidar beam but on a slant path at a different height.[14] In determining the effective turbulence levels for the experiment, we took these differences in the paths into account.[8]

A. RMS Noise

The simulation for comparison of RMS noise with experiment employed a 1024 x 1024 array and five propagation steps. A total of 100 realizations were run for each turbulence level. The signal was integrated over an annulus that was the same size and configuration as our experimental receiver. Independent speckle realizations were modeled in addition to independent turbulence realizations. The turbulence level (C_n^2) was simulated as uniform over the propagation path.

The model predictions for the combined effects on single-shot RMS noise and comparison to experimental results appear in Figure 2 and Figure 3 for the two ranges mentioned above. The two laser lines we used for this experimental comparison were chosen because of their negligible atmospheric absorption under normal operating conditions. The model, which neglects atmospheric absorption, accurately predicts the level of single-shot RMS noise for our annular aperture. It also correctly predicts the trend of increasing noise with increasing C_n^2.

B. Intensity Probability Distribution

We also compared the intensity probability distributions produced by the simulation with those measured in the experiment for varying turbulence conditions. In comparing these distributions we used the approximate Gamma distribution as a means of quantifying changes with turbulence. In using this distribution, we expect a deviation from theoretical predictions.[1]

Figure 4 shows fitted M values for both the simulation and experiment for a range of turbulence values. The simulation employed 1000 realizations with a 512 x 512 array and five propagation steps. In both the simulation and experiment there is a trend of decreasing M for increasing turbulence. The trend is a further validation of the consistency between the simulation and experiment. There are occasionally, however, additional noise sources in the experiment that are not modeled in the simulation. Deviations in M value have also been measured in other experiments.[15]

5. SIMULATION STUDIES

We have conducted some simulation studies to learn more about the reflective speckle-atmospheric turbulence interaction and as well as limitations of the simulation. These studies also serve to illustrate the utility of our model.

A. Variation of Array Size

The array or grid size is very important since larger arrays provide greater transverse spatial resolution. Since the optimization of the pixel size obeys the relationship, $\delta x = \sqrt{\lambda L / N}$, a larger array also results in a larger grid area. These improvements in resolution and grid size reduce aliasing effects inherent in Fourier transform techniques.[7] These simulations were done by considering an "original" grid size to be assessed. The propagation was conducted using pixel sizes for the "original" grid but propagating in a "new" grid that was twice the size of the "original." In this way, the spatial resolution was held at the "original" level providing a better overall picture of the aliasing effect in the receiver plane in the "new" larger grid. Once the round trip propagation progressed back to the receiver plane, the energy outside the "original" grid was compared to the total energy propagated. This analysis provides a quantification of the amount of energy that is unrealistically reflected back into the "original" grid when it is used. Figure 5 is a plot of the energy aliased outside a given grid versus "original" grid size for zero turbulence. As expected, there is a decrease in the aliasing ratio with increasing "original" grid size. The beam divergence also plays a role since larger beams in the target plane result in greater aliasing back at the receiver plane.

The effect of turbulence on this aliasing is also of interest. Figure 6 is a comparison of the aliasing effect for several grid sizes under increasing turbulence conditions. The ratio has more variation with increasing turbulence as indicated by the increasing error bars for the larger grids. There is a slight trend of a decrease in the aliasing effect with increasing turbulence and is due in part to a backscattered intensity enhancement that we shall explore in the next section.

B. Intensity Enhancement

Earlier studies have provided evidence of an enhancement of intensity in the backscatter of a laser beam through atmospheric turbulence. Previous work has included backscatter through a single phase screen after reflection from a mirror.[16] Other analytical work examined the round trip passage through turbulence after scattering from a rough target.[17] Experimental work used a turbulent cell as a distorting source to approximate the effect of single phase screen after reflection from a mirror.[18]

Simulation studies of this effect show a definite enhancement in the center of the receiver field with a peak width on the order of the transmitter output beam width. Figure 7 shows a comparison of the backscatter intensity enhancement for several values of the number of phase screens. The 20 phase screen case exhibits the greatest enhancement. This is due to the fact that within the limitations of the Huygens-Fresnel propagation scheme, the 20 phase screen case more closely models the reality of the turbulent propagation path. Increases of phase screens up to 40 screens showed no greater enhancement and larger increases actually exhibited a drop below the 20 phase screen value. This is an indication that simulations using the larger number of phase screens may have exceeded the limits of the model. The expression quantifying the maximum number of propagation steps, Equation (9), is an approximation. The assumptions that lead to this expression are order of magnitude estimates that for this propagation geometry predicted the maximum number phase screens at roughly six times the value of 20 determined as optimum for the intensity enhancement effect.

We have also looked at the case where the turbulence is not "frozen" (different phase screens for forward and reverse propagation). Figure 8 shows a comparison for two 20 phase screen cases. In each case the intensity was summed for annular radii over 100 realizations. Both cases have the same level or strength of turbulence. The pulses that traversed the same phase screens on both paths resulted in a definite enhancement in intensity with a central peak. The pulses that traversed new or different turbulent phase screens on the return path do not exhibit this sharp central peak. The new phase

screens traversed on the return path are statistically similar to the phase screens traversed on the outgoing path but represent a different realization of turbulence. Both cases do exhibit the peaking toward the center over a wide portion of the receiver grid. This is due in part to aliasing and possibly another broader component of the enhanced backscattered intensity.

In Figure 9 we see the increasing trend of the intensity enhancement with increasing turbulence. The results shown are the average of 1000 realizations. The narrow central peak definitely grows with increasing levels of atmospheric turbulence.

The lidar system compared to simulation in this work has an obscuring turning mirror that is a little larger than the transmitter output beam. Most of the backscatter enhancement intensity is lost when the pulse returns. However, some of the enhancement is integrated by the receiver and will result in increasing values of return signal for increasing levels of turbulence for this geometry.

C. Intensity Probability Distributions and Variation of Propagation Step Size

The variation of step size and its effect on intensity enhancement prompted investigation of step size variation on intensity probability distributions. Figure 10 presents a comparison of *M* value versus RMS noise for data obtained from experiment and simulation at various turbulence levels. There is also a comparison to free space speckle theory which is of the approximate form[1]

$$M \cong \left(\frac{Signal}{Noise} \right)^2_{rms} . \qquad (14)$$

The trend of decreasing M value with increasing RMS noise for this lidar geometry is apparent. Also evident is the deviation from the theory of Equation (14) at the higher values of RMS noise.

The simulations were conducted for 1000 realizations and a 512 x 512 array. Both simulations schemes used the same five levels of turbulence. However, the 20 phase screen case resulted in lower noise than the 5 phase screen case due at least in part to the greater intensity enhancement in the 20 phase screen case. The 20 phase screen case also shows a slightly better agreement with experimental results.

6. CONCLUSIONS

For the lidar geometry of our experiment, the single-shot RMS noise is 40-50% larger under the higher turbulence conditions. The impact of this trend for lidar operations is significant. Even if multi-shot averaging is used to improve the lidar measurement, the initial noise level will be markedly higher for conditions of increased turbulence requiring longer averaging times to reach a given noise level. Our model accurately shows the level of RMS noise for our finite aperture. It also produces the trend of increasing RMS noise with increasing turbulence level (C_n^2) for our lidar geometry. The model displays the trend of changing intensity probability distributions with varying levels of atmospheric optical turbulence.

Simulation studies showed that an increase in grid sizes resulted in a decrease in aliasing of energy off the propagation grid in the receiver plane. Larger beam profiles on target also resulted in greater aliasing back in the receiver plane. The simulation studies also provided further evidence of a backscattered intensity enhancement in the receiver plane. This enhancement increased for increasing levels of turbulence up to the limit of the weak turbulence regime. Intensity probability distributions showed a dependence on the size of the propagation step. Smaller steps showed greater agreement with experimental values than did longer steps. Both, however, displayed the experimentally determined trend with increasing RMS noise and a deviation from vacuum speckle theory.

These results provide experimental verification for our modeling of the combined effects of atmospheric optical turbulence and reflective speckle. The results also emphasize, for this lidar geometry, the impact of increased turbulence levels on lidar operations and provide motivation for further study.

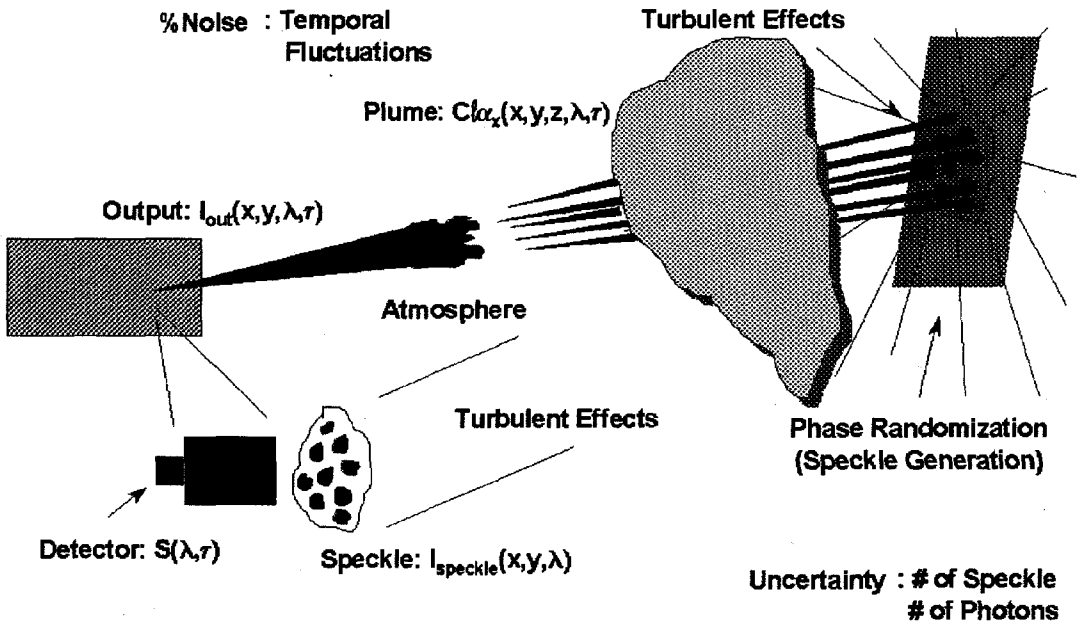

Figure 1. Hard target reflection scheme of lidar highlighting effects of the atmosphere and the target on the return signal.

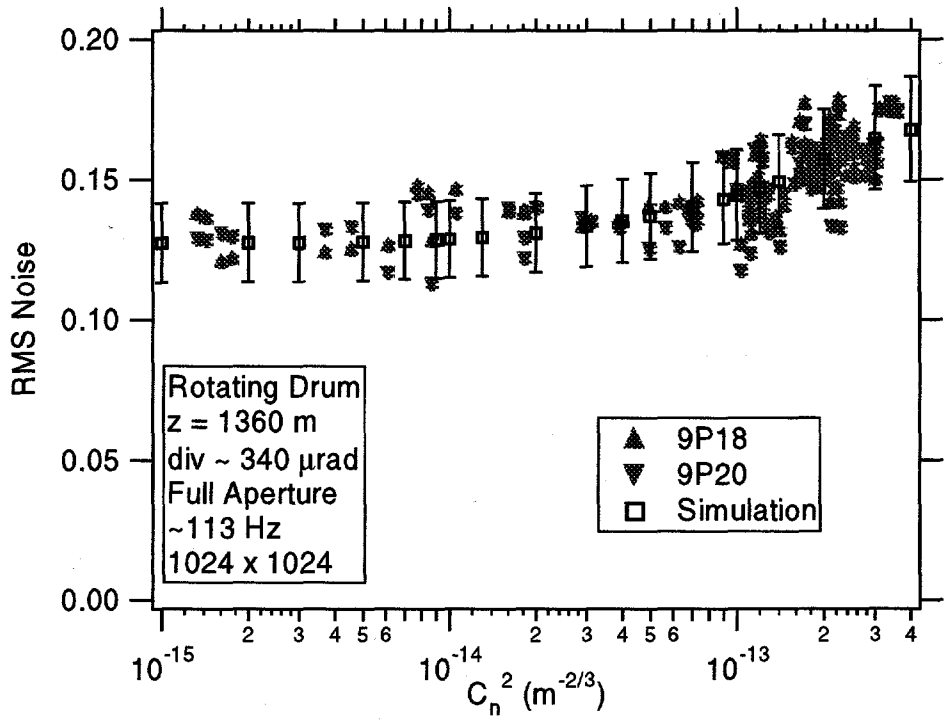

Figure 2. Comparison of simulation with experiment for a target at 1360 m. The beam divergence was approximated as ~340 µrad. The receiver is annular with an area of ~ 0.06 m^2. The simulation grid was 1024 x 1024. Five propagation steps were used for each leg of the round trip path. The propagation path was assumed horizontal with a uniform turbulence level along the path.

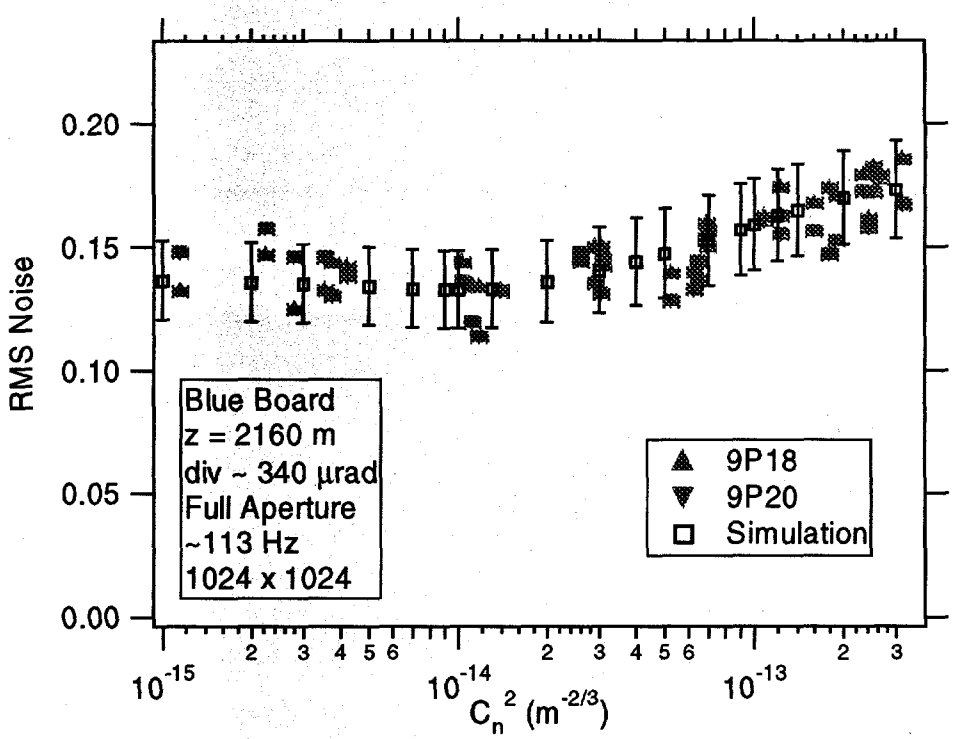

Figure 3. Comparison of simulation with experiment for a target at 2160 m. The beam divergence was approximated as ~340 µrad. The receiver is annular with an area of ~ 0.06 m^2. The simulation grid was 1024 x 1024. Five propagation steps were used for each leg of the round trip path. The propagation path was assumed horizontal with a uniform turbulence level along the path.

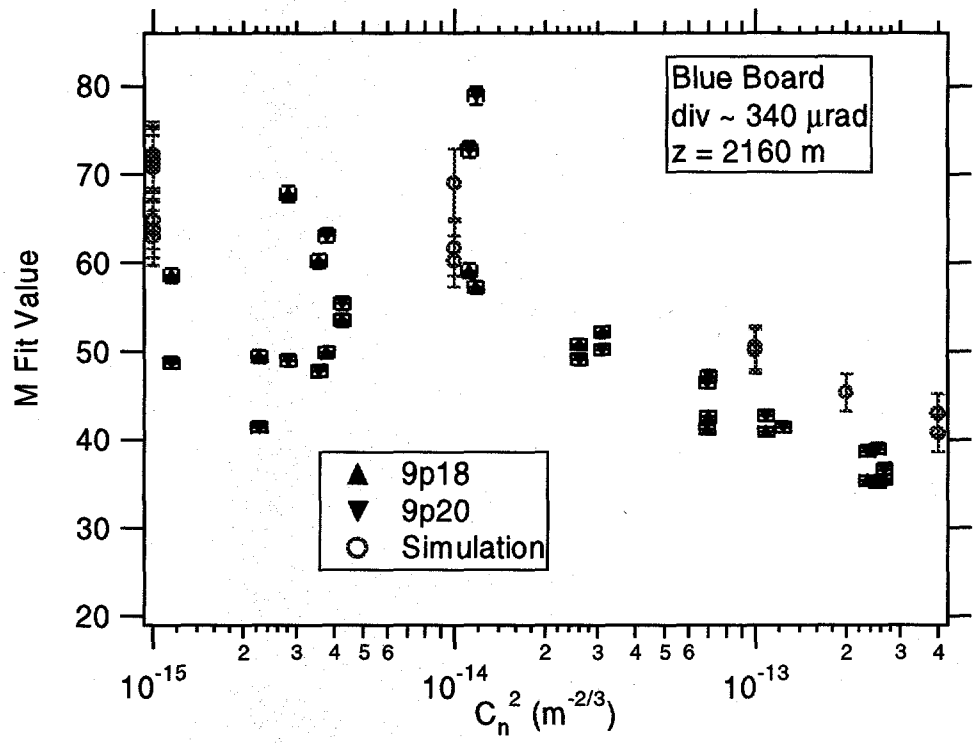

Figure 4. *M* values for experiment and simulation over a range of turbulence levels.

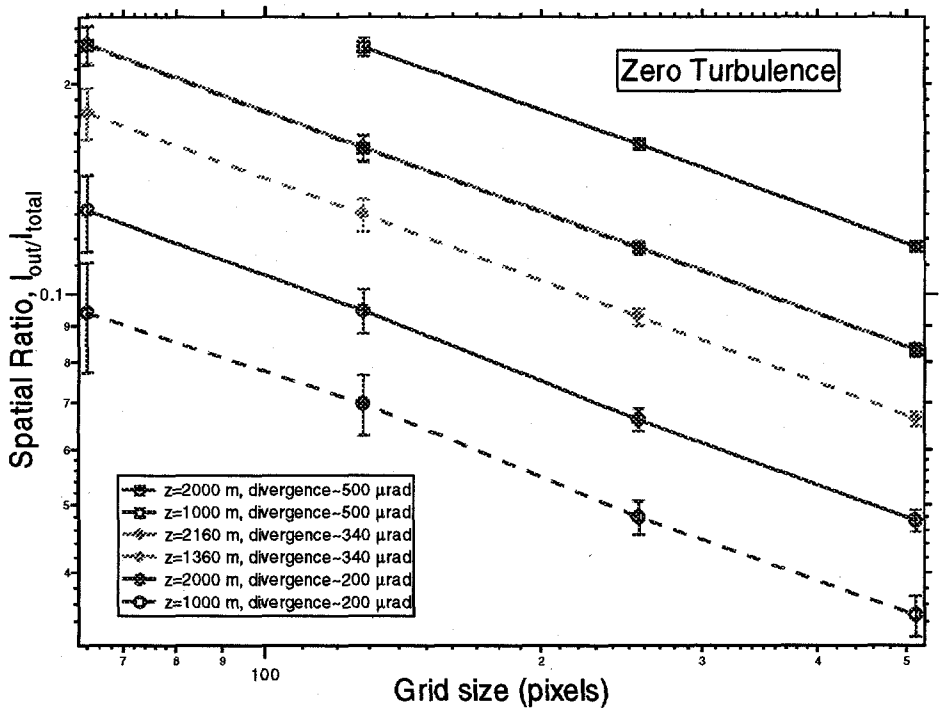

Figure 5. Ratio of irradiance outside a given grid to the total integrated irradiance versus grid size for zero turbulence conditions.

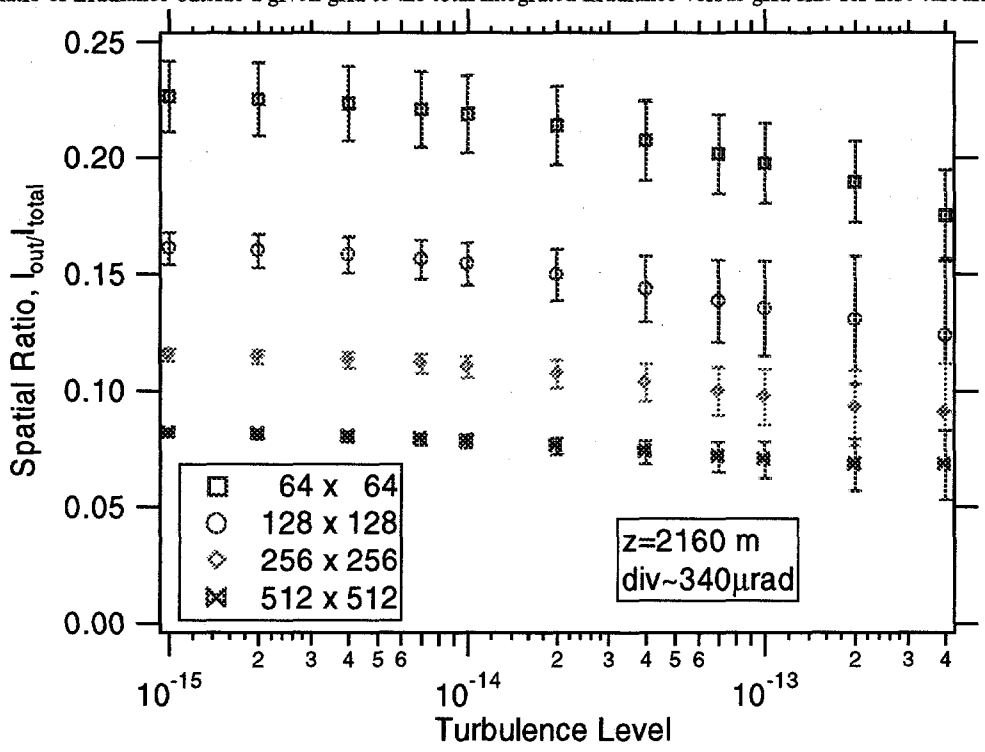

Figure 6. Ratio of irradiance outside a given grid to the total integrated irradiance versus turbulence level for several grid sizes.

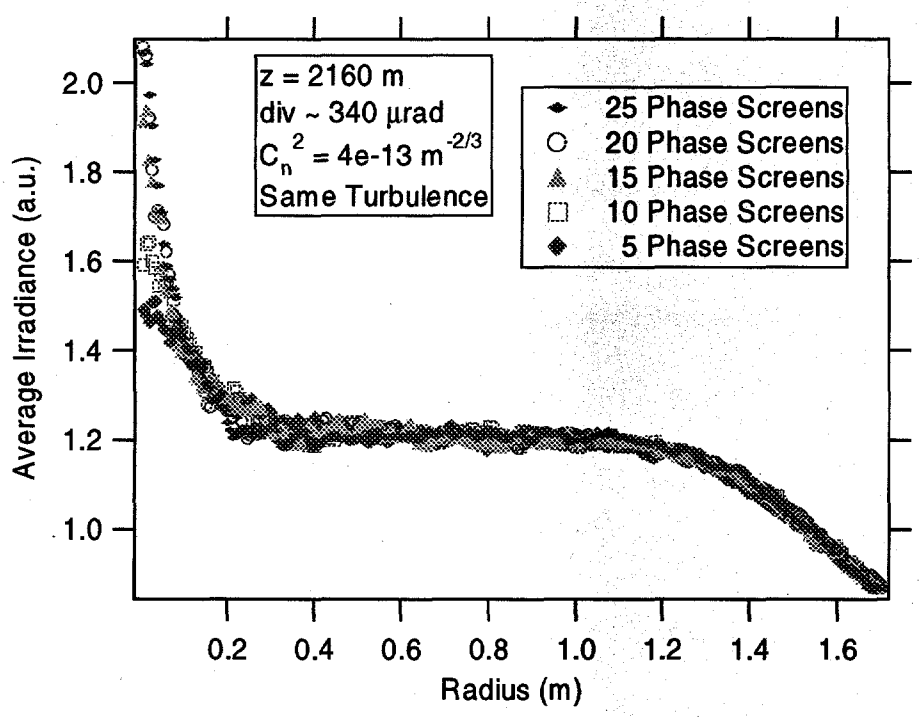

Figure 7. Average irradiance from simulation versus radius from center of grid for several propagation step sizes.

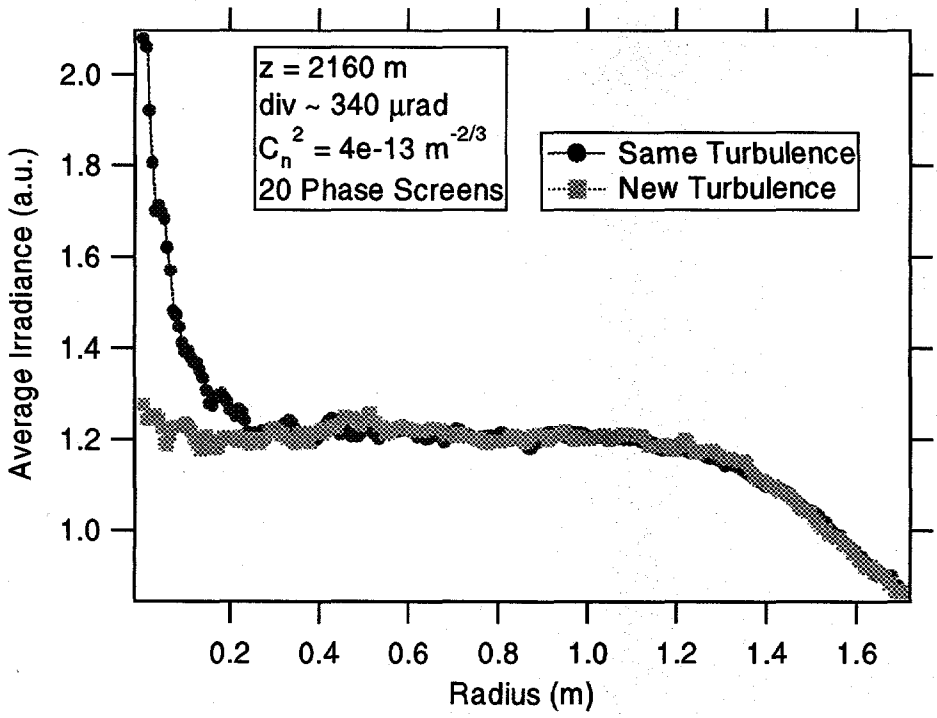

Figure 8. Comparison of average irradiance versus radius from center of grid for return through the same phase screens and different but statistically identical phase screens.

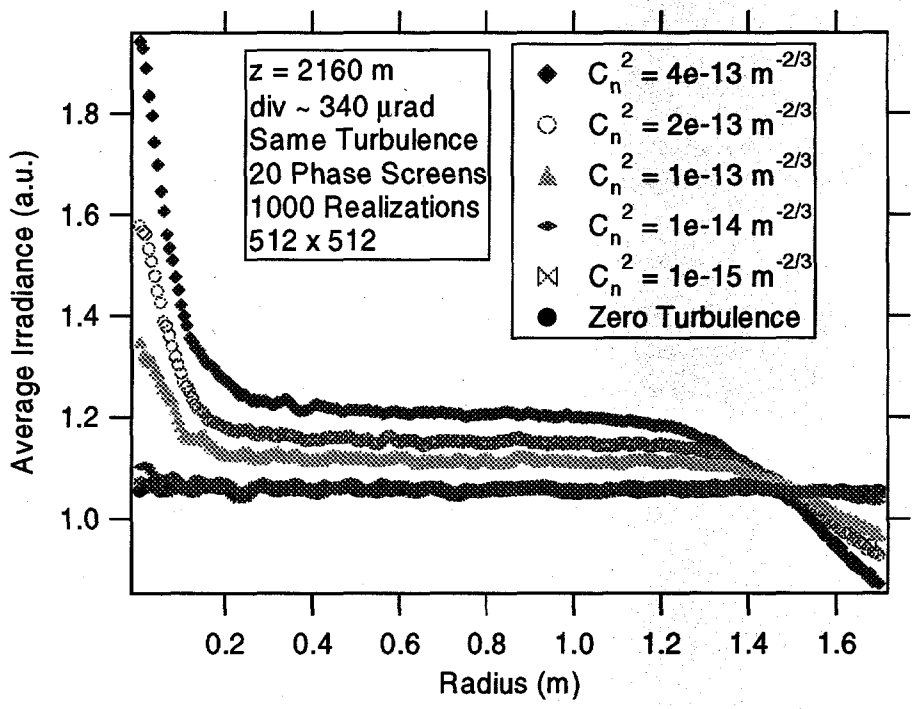

Figure 9. Average irradiance versus radius from center of grid for several turbulence levels.

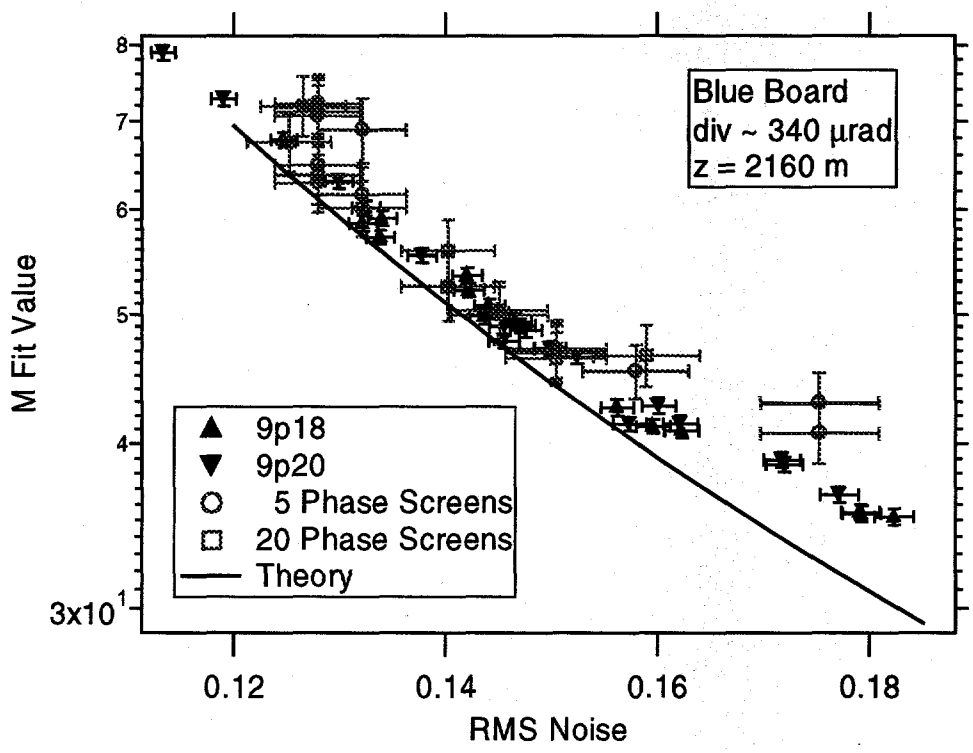

Figure 10. Comparison of *M* value versus RMS noise for experiment, varying simulation step sizes and vacuum speckle theory.

7. ACKNOWLEDGEMENTS

This work was part of a large lidar project with many important team members and we wish to thank all of them. The authors would also like to acknowledge the cooperation of the DOE Remote Sensing Laboratory, Nellis Air Force Base and Air Force Research Laboratory. This research was fully supported by the U.S. Department of Energy under contract W-7405-ENG-36.

8. REFERENCES

[1] D.H. Nelson, R.R. Petrin, E.P. MacKerrow, M.J. Schmitt, C.R. Quick, A. Zardecki, W.M. Porch, M.C. Whitehead and D.L. Walters, "Wave optics simulation of atmospheric turbulence and reflective speckle effects in CO_2 differential absorption LIDAR (DIAL)," *Airborne Laser Advanced Technology*, **3381**, 147-158, SPIE, Bellingham, WA (1998).

[2] D.H. Nelson, D.L. Walters, E.P. MacKerrow, M.J. Schmitt, C.R. Quick, W.M. Porch and R.R. Petrin, "Wave optics simulation of atmospheric turbulence and reflective speckle effects in CO_2 lidar," submitted to Applied Optics.

[3] J.F. Holmes, "Speckle propagation through turbulence: its characteristics and effects," *Proc. SPIE*, **410**, 89-97 (1983).

[4] M.V. Klein and T.E. Furtak, *Optics*, John Wiley & Sons, New York, 1986.

[5] J.W. Goodman, *Introduction to Fourier Optics* (McGraw-Hill, New York, 1968).

[6] D. L. Knepp, "Multiple phase-screen calculation of the temporal behavior of stochastic waves," *Proc. IEEE* **71**, 722-737 (1983).

[7] C.A. Davis and D.L. Walters, "Atmospheric inner-scale effects on normalized irradiance variance," *Appl. Opt*, **33**, 8406-8411 (1994).

[8] R.R. Beland, "Propagation through atmospheric turbulence," *The Infrared Electro-optical Systems Handbook*, Vol. 2, SPIE, Bellingham, WA, 157-232, 1993.

[9] J.M. Martin and S.M. Flatté, "Simulation of point-source scintillation through three-dimensional random media," *J. Opt. Soc. Am. A*, **7**, 838-847 (1990).

[10] J.M. Martin and S.M. Flatté, "Intensity images and statistics from numerical simulation of wave propagation in 3-D random media," *Appl. Opt*, **27**, 2111-2126 (1988).

[11] R.E. Hufnagel, "Propagation through atmospheric turbulence," *The Infrared Handbook*, Chapter 6, Environmental Research Institute of Michigan, Ann Arbor, MI, 1985.

[12] J.W. Goodman, "Statistical properties of laser speckle patterns," *Laser Speckle and Related Phenomena*, 2nd ed,. J. Dainty, Ed., Springer-Verlag, New York, 1984.

[13] E.P. MacKerrow and M.J. Schmitt, "Measurement of integrated speckle statistics for CO_2 lidar returns from a moving, nonuniform, hard target," *Appl. Opt*, **36**, 6921-6937 (1997).

[14] T. Wang, G.R. Ochs and S.F. Clifford, "A saturation-resistant optical scintillometer to measure C_n^2," *J. Opt. Soc. Am.*, **68**, 334-338 (1978).

[15] A. Dabas, P.H. Flamant and P. Salamitou, "Characterization of pulsed coherent Doppler LIDAR with the speckle effect," *Appl. Opt*, **33**, 6524-6532 (1994).

[16] G. Welch and R. Phillips, "Simulation of enhanced backscatter by a phase screen," *J. Opt. Soc. Am. A.*, **7**, 578-584 (1990).

[17] J.F. Holmes, "Enhancement of backscattered intensity for a bistatic lidar operating in atmospheric turbulence," *Appl. Opt*, **30**, 2643-2646 (1991).

[18] B.S. Agrovski, A.N. Bogaturov, A.S. Gurvich, S.V. Kireev and V.A.Myakinin, "Enhanced backscattering from a plane mirror viewed through a turbulent phase screen," *J. Opt. Soc. Am. A.*, **8**, 1142-1147 (1991).